

Dual Active Site of the Azo and Carbonyl-Modified Covalent Organic Framework for High-Performance Li Storage

Genfu Zhao,[§] Yuhao Zhang,[§] Zhihui Gao, Huani Li, Shuming Liu, Sheng Cai, Xiaofei Yang, Hong Guo,^{*} and Xueliang Sun^{*}



Cite This: *ACS Energy Lett.* 2020, 5, 1022–1031



Read Online

ACCESS |



Metrics & More

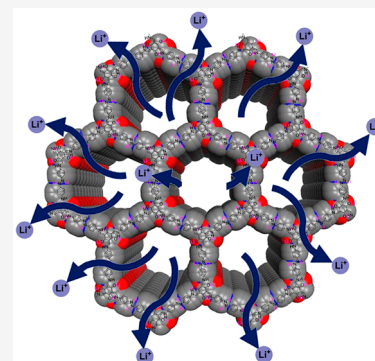


Article Recommendations



Supporting Information

ABSTRACT: Organic electrode materials play a crucial role in environmentally friendly and sustainable lithium-ion batteries (LIBs) due to their abundance, high theoretical capacity, inexpensiveness, and recyclability. However, critical issues such as fewer redox-active sites and poor structural stability limit their extensive application in LIBs. Herein, a unique covalent organic framework (Tp-Azo-COF) with a dual active site of N=N and C=O is designed and successfully applied as the anode material for LIBs. Benefiting from its abundance of active sites, large conjugate structure, large surface area, and accessible Li⁺ transport channels, the Tp-Azo-COF anode materials present high electrochemical kinetics and structural stability. The assembled LIBs deliver a specific capability of 305.97 mAh g⁻¹ at a current density of 1000 mA g⁻¹ after 3000 cycles. This work may inspire avenues for the development of advanced organic materials of inexpensive, sustainable, and durable rechargeable batteries.



Lithium-ion batteries (LIBs), as fundamental energy storage and conversion devices, play a crucial role in handy vehicles.^{1–3} Nonetheless, several environmental challenges, including heavy metal pollution, water pollution, and soil pollution, pose concerns with respect to the extensive utilization of LIBs.^{4–6} These challenges can promote the exploration of newly environmentally friendly and sustainable materials. Accordingly, developing and fabricating high-performance, sustainable, and green electrode materials are extraordinarily crucial for the application of LIBs.

Organic compounds exhibit abundant attractive properties, including their abundance, low density, flexibility, inexpensiveness, sustainability, and highest occupied molecular orbital (HOMO) or lowest unoccupied molecular orbital (LUMO) energetics, and thus are easily engineered at the molecular level.^{7–10} In particular, heteroatom-containing aromatic compounds, with a lone pair of electrons, exhibit superior redox activity and can be utilized as electroactive organic electrodes to meet the growing demand for energy storage and conversion.^{11–14} So far, plentiful organic compounds have been explored as the high-activity LIB electrodes, such as organic carbonyl (C=O) compounds,^{15–17} imine (C=N) compounds,^{18–20} polymers, and organic radical species.^{21–25} In particular, a new organic compound containing an azo (N=N) group has been explored and successfully applied for lithium- and sodium-ion batteries.^{26–28} Despite their promise, the extensive application of these organic compounds in LIBs

is still limited by their intrinsic drawbacks. For instance, these organic compounds possess restricted active sites, limiting the improvement of their electrochemical kinetics. Moreover, the solubility of organic compounds in the electrolyte and inferior crystallinity give rise to poor cycling stability and a rapid decline in capacity, as well. Taking these features into consideration, researchers have spent a tremendous amount of effort to improve the cycling stability and electrochemical kinetics of organic compound-based LIBs. Three strategies can be identified: (1) covalently attaching the electroactive organic molecule to a conductive backbone, (2) polymerizing the redox-active compounds to reduce the dissolution, and (3) forming a salt with organic carboxylic acid compounds. These approaches have proven to exhibit positive effects on alleviating the dissolution of organic compounds into electrolytes. However, a high conductive carbon content of >50 wt % should be introduced into the electrode to build the electronic conductive networks for the electrochemical reaction of organic compounds, thus leading to unsatisfied energy density.

Received: January 10, 2020

Accepted: March 5, 2020

Published: March 5, 2020

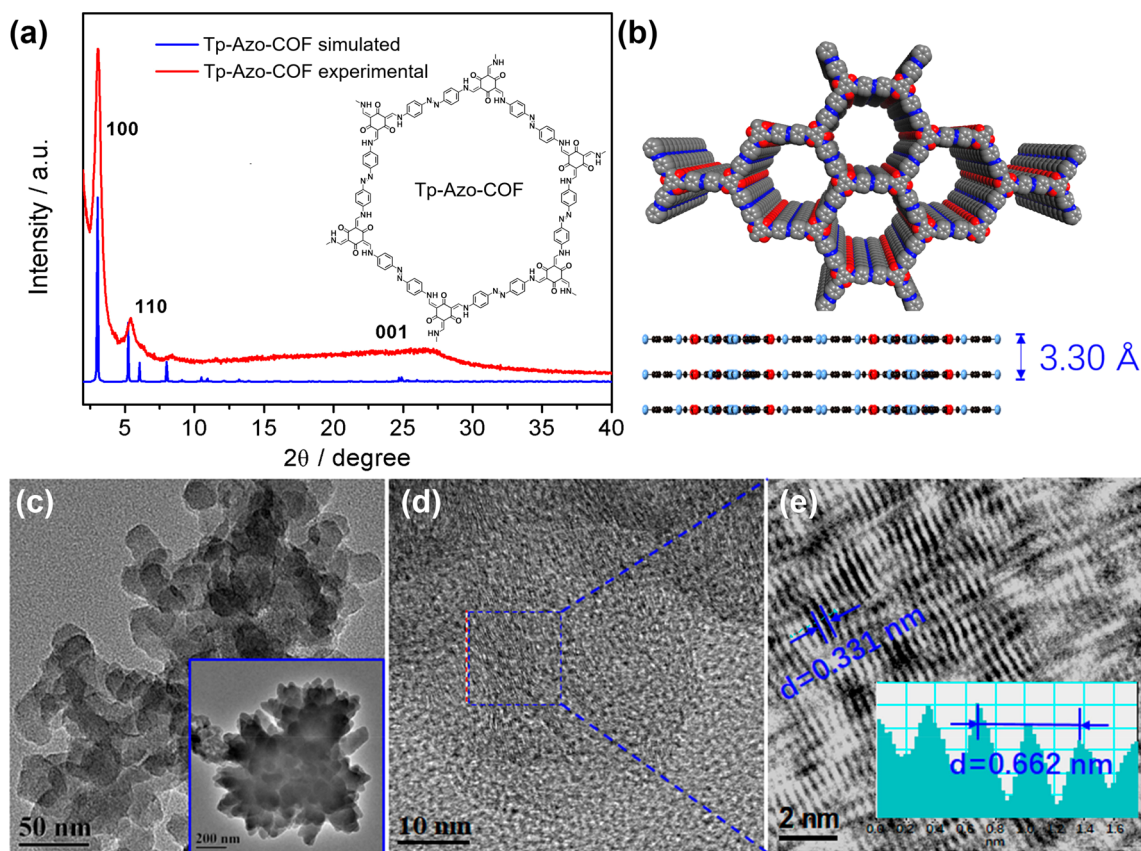


Figure 1. (a) PXRD patterns of experimental and simulated eclipsed patterns of Tp-Azo-COF. (b) Schematic representation of the preparation Tp-Azo-COF. (c–e) TEM images at various magnifications.

Accordingly, designing and constructing excellent chemical and physical stability, high crystallinity, and affluent and multifarious sites to reversibly react with Li^+ are essential and challenging for fast charge–discharge and outstanding cycling stability.^{29,30}

Covalent organic frameworks (COFs) possess a prominent structural skeleton with high porosity, high crystallinity, ease of chemical modification, and excellent stability under various harsh conditions; thus, they have attracted an extensive amount of attention in recent years.^{31–33} Among them, a two-dimensional (2D) COF has been used in important applications in energy storage and conversion.^{34–36} Lu et al. reported the β -ketoenamine- and anthraquinone-linked 2D COF had rich carbonyl ($\text{C}=\text{O}$) groups to react with Na ion and showed high capacity acting as the anode material in sodium-ion batteries (SIBs).³⁷ Feng et al. reported a 2D polyarylimide-based COF as the anode material in LIBs that presented strong rate capability and cycle stability.³⁸ Moreover, El-Kaderi reported porous azo-linked ($\text{N}=\text{N}$) polymers exhibited electrochemical redox activity.²⁶ This preminent research implies that a COF can act as an ideal electrode material for LIBs or SIBs. While few advances of complex composites with other materials of COFs in LIBs have been achieved,^{37,38} the deficiency in LIBs should attract attention, with features such as limited active centers, low capacities, and short cycles.

Herein, a dual redox-active site of $\text{C}=\text{O}$ and $\text{N}=\text{N}$ chemically modified COF (Tp-Azo-COF) is proposed and successfully applied in LIBs. The strong π – π interactions among the 2D COF layers remarkably improve the electronic

conductivity and reduce the COF's solubility in electrolytes. Additionally, the introduction of $\text{C}=\text{O}$ and $\text{N}=\text{N}$ dual redox-active sites enhances the electrochemical activity and capacity significantly. Benefiting from the enhanced electronic conductivity, reduced level of electrode material dissolution, and improved electrochemical activity, the LIBs assembled with Tp-Azo-COF electrodes display superior capacity output and predominant cycling stability, with values of $305.97 \text{ mAh g}^{-1}$ and roughly 100% capacity retention, respectively, after 3000 charge–discharge cycles at a current density of 1000 mA g^{-1} . This work will open a new window for the rational design of high-performance organic compound-based LIBs.

Tp-Azo-COF is effortlessly made by condensing 4,4'-azodianiline (Azo) and 1,3,5-triformylphloroglucinol (Tp) using 1,4-dioxane as the solvent according to previous reports (Scheme S1).^{39,40} The crystalline structure of Tp-Azo-COF was studied by powder X-ray diffraction (PXRD). Figure 1A exhibits the experimental PXRD pattern of Tp-Azo-COF, and the pattern matches well with the simulated pattern of the AA structure. Furthermore, experimental PXRD exhibits a sharp diffraction peak at 2θ of $\sim 3.2^\circ$, which is attributed to the (100) facet. At the same time, peaks at $\sim 5.41^\circ$ and 27.2° can be ascribed to the (110) and (001) planes, respectively, of Tp-Azo-COF, and the (001) plane is generated from π – π stacking between the Tp-Azo-COF layers.^{39,40} These peaks confirm the high crystallinity of the as-prepared Tp-Azo-COF. The porosity of Tp-Azo-COF is determined by the N_2 sorption–desorption measurements at 77 K, displaying a regular IV-type N_2 adsorption isotherm (Figure S1). The pore distribution is analyzed and calculated on the basis of the nonlocal density

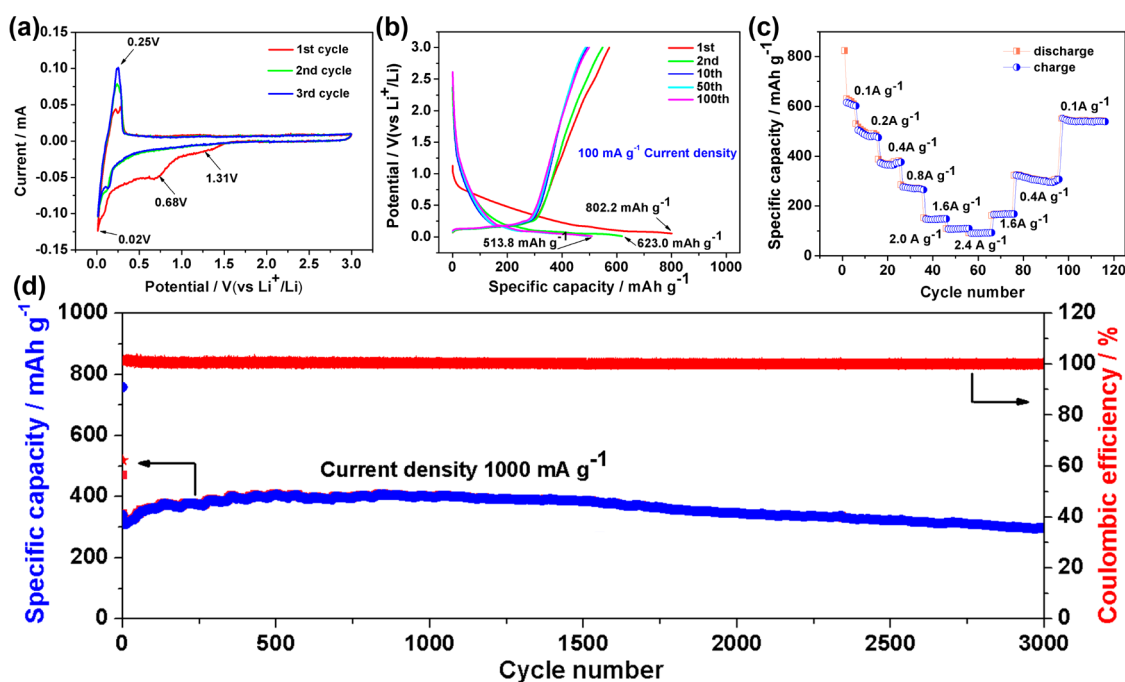


Figure 2. (a) CV curves of Tp-Azo-COF at 0.1 mV s^{-1} . (b) Galvanostatic charge–discharge curves of the Tp-Azo-COF anode material at 0.3 C . (c) Rate capability performance at different current densities of $0.1\text{--}2.4 \text{ A g}^{-1}$. (d) Long-term cycling stability of Tp-Azo-COF at 1000 mA g^{-1} .

functional theory. As illustrated in Figure S2, Tp-Azo-COF displays a sharp and small cavity diameter of $\sim 2.6 \text{ nm}$, resulting in a large specific surface area of $632 \text{ m}^2 \text{ g}^{-1}$. The surface area is smaller than that reported previously,³⁹ which might be caused by the purification process. In this regard, we can conclude that the as-prepared Tp-Azo-COF is a crystalline 2D material with a high porosity and a large specific surface area, which is beneficial for capturing and transferring Li ion during the charge–discharge process.^{38,41}

The microstructure of Tp-Azo-COF was examined by transmission electron microscopy (TEM), and the results are shown in Figure 1c–e. Tp-Azo-COF exhibits a flowerlike structure with aggregation of a good deal of petals.³⁹ More importantly, the well-ordered crystalline structure of Tp-Azo-COF is also proven by the high-resolution TEM image (Figure 1e). It is easy to see the interplanar distance of 0.331 nm from the d spacing distribution, which strongly agrees with the theoretical value of 0.330 nm (Figure 1b). Moreover, scanning electron microscopy (SEM) further confirms this flowerlike morphology, and EDS mapping demonstrates that the C, N, and O elements are uniformly dispersed (Figure S3). Fourier transform infrared (FT-IR) spectrometry is implemented to assess the unique C=O chemical group of the β -ketoenamine. An obvious peak at 1618 cm^{-1} is observed,^{42–44} implying the successful formation of β -ketoenamine between Tp and Azo (Figure S4). Raman spectroscopy, as the results show, is applied to characterize the breathing vibration of the N=N group. As depicted in Figure S5, the characteristic N=N peak of Tp-Azo-COF can be distinctly found at 1450 cm^{-1} , which indicates that the result strongly agrees with the structure of synthetic Tp-Azo-COF.⁴⁵ Thermogravimetric analysis (TGA) is carried out to study the thermal stability of Tp-Azo-COF (Figure S6); an obvious weight loss occurs after $300 \text{ }^\circ\text{C}$, implying its high thermal stability.⁴⁶

The electrochemical behavior of Tp-Azo-COF is explored in the working voltage window of $0.01\text{--}3.0 \text{ V}$ within CR2016 coin cells, where Li foil is chosen as the counter/reference electrode and the active material loading in the anode is $\sim 3.15 \text{ mg cm}^{-2}$. Cyclic voltammetry (CV) with scan rate of 0.05 mV s^{-1} is carried out to evaluate the electrochemical reaction kinetics. As presented in Figure 2a, during the negative scan in the first cycle, the CV curve displays three cathodic peaks at 1.31 , 0.68 , and 0.02 V (vs Li^+/Li), corresponding to a multistep Li intercalation process followed by the electrochemical reduction of Tp-Azo-COF. The low potential value for Li intercalation might stem from the fact that various materials are used as the counter electrode.^{37,38} The weak peak at 1.31 V (vs Li^+/Li) can be ascribed to the reduction reaction of surface-active materials, which is caused by the SEI. The apparent reduction peak centered at 0.68 V gradually slows, revealing the occupation of Li at the C=O and N=N positions and formation of strong ionic bonds such as Li–O– and Li–N– bonds. The cathodic peak, which appeared at 0.02 V (vs Li^+/Li), corresponds to the loading of Li in the cavity of Tp-Azo-COF. Subsequently, during the positive scan, the anodic peak located at 0.25 V is observed, corresponding to the reversible oxidization of active groups in Tp-Azo-COF. In the following cycles, the CV curves almost overlap, suggesting the highly reversible reaction and excellent cycling stability of Tp-Azo-COF-based LIBs.

To investigate the efficiency of the prepared electrodes in reversible Li^+ storage, the galvanostatic Li^+ -ion intercalation/deintercalation research is implemented with potentials of $0.01\text{--}3.0 \text{ V}$ (vs Li^+/Li) at a current density of 100 mA g^{-1} . The galvanostatic discharge–charge profiles of the first, second, 10th, 50th, and 100th cycles are shown in Figure 2b. In the first discharge profile, a wide and stable discharging plateau that started from 0.68 V with a high capacity of 802.2 mAh g^{-1} can be observed. In the second cycle, reversible capacities of

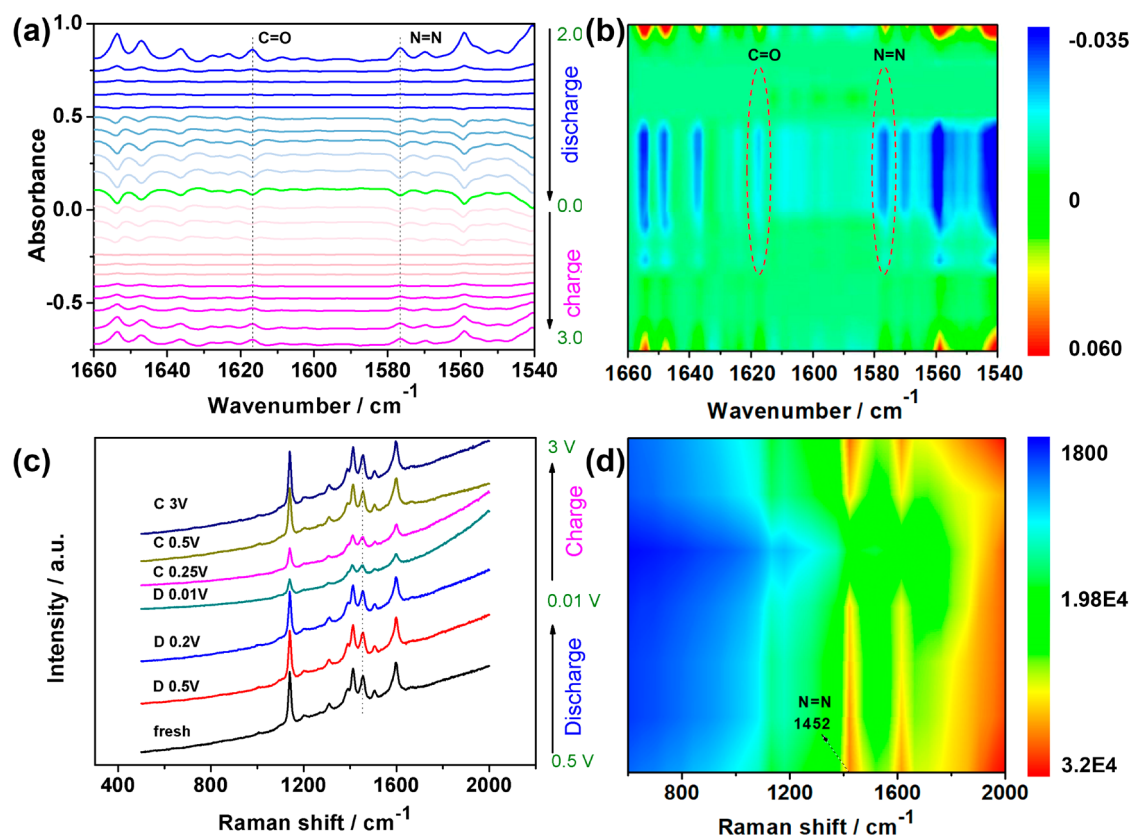


Figure 3. (a) In situ FT-IR spectral changes of the as-made electrode sample at different discharge states. (b) Contour and response surface analysis corresponding to the discharge process. (c) Raman spectroscopy to study the redox mechanism of Tp-Azo-COF. (d) Contour and response surface analysis corresponding to the discharge–charge process.

>623.0 mAh g⁻¹ are achieved and a discharge capacity plateau at ~0.02 V is presented, which strongly agrees with the previous CV curves. The capacity loss of ~179.8 mAh g⁻¹ from the first cycle to the second cycle can be ascribed to the contribution of SEI formation. The discrepancy in capacity between theoretical analysis and experimental measurement is attributed to the inaccessible reactive sites of N=N and C=O units on the host framework, because the reactive sites can be reduced by the electrostatic repulsion interactions between the near N atom of azo bonds and the O atom of C=O.³⁸ In addition, Tp-Azo-COF is a two-dimensional material and can form a stacking structure between adjacent COF layers, which might conceal the reactive sites.^{37,38,41} Subsequently, negligible changes can be observed in the charge–discharge curves of the subsequent cycles, demonstrating the occurrence of stable and reversible electrochemical reaction. Even after long-term cycling of >100 cycles, a high specific capacity of ~513.8 mAh g⁻¹ is still maintained at 100 mA g⁻¹ (Figure 2b), proving its outstanding cycling stability and high capacity output.

Rate capability, as the crucial parameter for quantifying the performance of batteries, has been widely adopted to evaluate capacity retention with elevated current densities. The rate performance of the LIBs assembled with Tp-Azo-COF electrodes is estimated under various current densities from 0.1 to 2.4 A g⁻¹, and the results are shown in Figure 2c. The electrode material Tp-Azo-COF generates a discharge specific capacity of 623.0 mAh g⁻¹ under a current intensity of 0.1 A g⁻¹ for the first few cycles. Despite the addition of high current densities, no appearance of relaxation between the cycles can be observed and the Tp-Azo-COF electrode material still

displays satisfied specific capacities: 494.49, 387.19, 292.71, 145.75, 108.6, and 90.76 mAh g⁻¹ for 0.2, 0.4, 0.8, 1.6, 2.0, and 2.4 A g⁻¹, respectively. After the current density is returned to 0.1 A g⁻¹, the Tp-Azo-COF electrode recovered a reversible capacity of 529.5 mAh g⁻¹, suggesting the highly structural stability under high current densities. The long-term cycling performance of Tp-Azo-COF is further investigated at a current density of 1 A g⁻¹ (Figure 2d). After 3000 cycles, a high capacity of >305.97 mAh g⁻¹ and almost 100% capacity retention and a high Coulombic efficiency of around 100% can be observed, demonstrating the Tp-Azo-COF anode material shows prominent ultrastability and sufficient reactive site utilization.³⁸ Generally, the electrochemical performance of the Tp-Azo-COF material in terms of capacity output, cycling stability, and rate performance is superior to those of other recently reported organic compounds in LIBs (Table S1).

To deeply understand the buried evolution process of the Tp-Azo-COF anode material during cycling, the cells after cycling are disassembled and the Tp-Azo-COF anodes are investigated by diverse characterization techniques. In situ FT-IR (Figure S7), as the available analytic technique, is introduced to understand the discharging process. As shown in Figure 3a, FT-IR spectroscopy of the pristine material reveals the characteristic absorbed peak at wavenumbers of 1618 and 1578 cm⁻¹, which are ascribed to the C=O and N=N groups,^{42,44} respectively. With the discharging depth increasing, the intensity of the FT-IR absorbance of the formed electrode increases gradually, implying that the active sites of C=O and N=N units are occupied and form strong ionic bonds such as Li–O– and Li–N– bonds during Li-ion

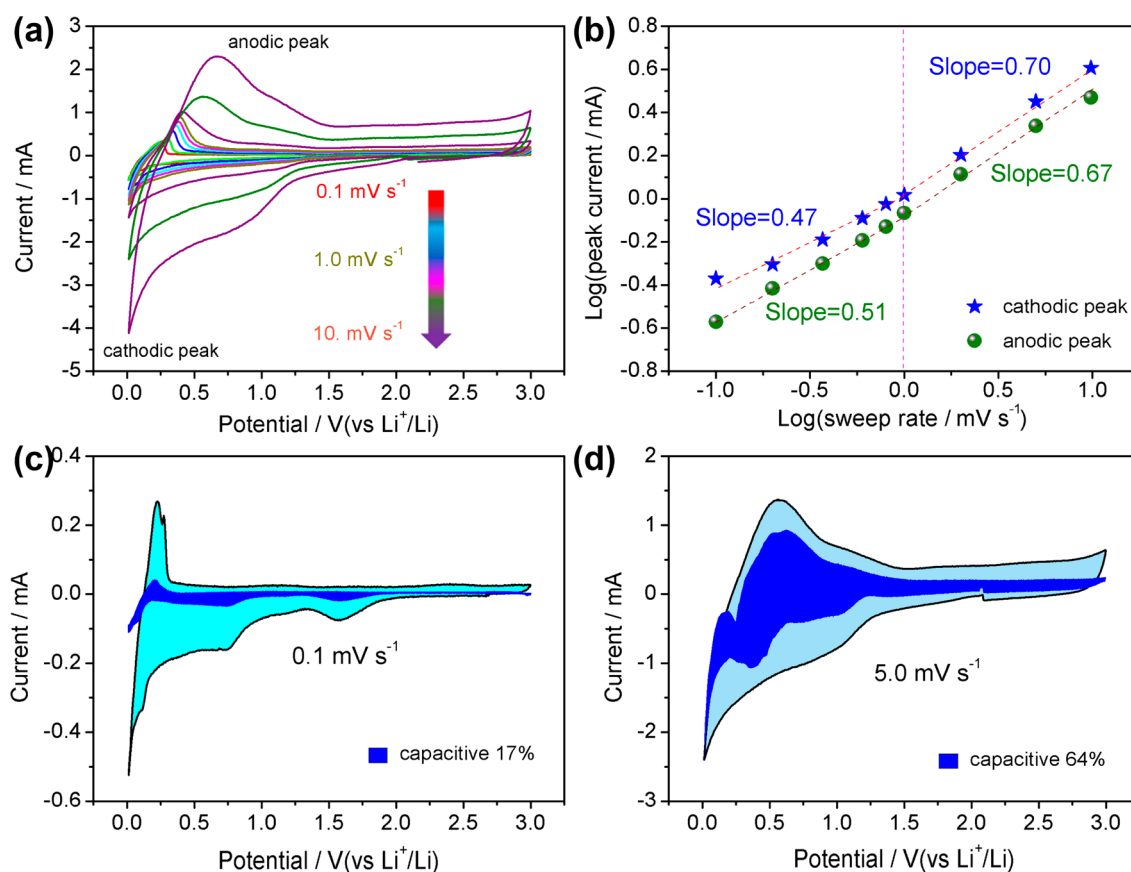


Figure 4. (a) CV curves of Tp-Azo-COF collected under different scan rates from 0.1 to 10 mV s^{-1} . (b) Plots of log current vs log scan rate to determine the slope values of different peaks. (c and d) Separation of capacitive and diffusion currents at 0.1 and 5 mV s^{-1} , respectively.

insertion.^{26–28,38,42} Interestingly, the intensity change of the FT-IR absorbance is the inverse of the intensity change of FT-IR transmittance, and the peak of FT-IR absorbance is upward. When samples are discharged to 0.01 V, the absorbed peaks at wavenumbers of 1618 and 1578 cm^{-1} have changed obviously, and the intensities of the absorbed peaks continuously increase with the decrease in discharge potential, implying the consumption of the active sites. When the anode material is charged to 3.0 V, the characteristic C=O and N=N groups appear. This process can be clearly reflected by the contour and response surface analysis corresponding to the discharge process (Figure 3b). Therefore, with the consumption of C=O and N=N active units, the changes in peak absorbance are from upward to downward. Moreover, in the charged process, the peak can appear, revealing the excellent high reversibility of the Tp-Azo-COF anode material. The changes of other peaks might be generated from the organic or inorganic matrix in the interface layer between the activity part and the electrolyte.²⁷

The reversible Li^+ insertion/extraction process is further confirmed by the Raman spectra. As shown in panels c and d of Figure 3, when the Tp-Azo-COF electrode is discharged to 0.01 V, the characteristic peak of the N=N group located at 1452 cm^{-1} almost disappears, which can be assigned to the consumption of N=N by Li^+ insertion.²⁶ In the subsequent charging process, we found that the N=N bond emerges again, further proving the high reversibility of the Tp-Azo-COF anode material in LIBs. Additionally, the PXRD patterns of Tp-Azo-COF after cycling tests show a similar profile (Figure S8), which can further certify the integrity of the framework. In particular, the PXRD patterns of as-made electrode material

Tp-Azo-COF do not have the characteristic peak at 3.2° (100 facet) by comparison with a fresh sample of Tp-Azo-COF. It is not caused by the change in the framework of Tp-Azo-COF but by the hiding of the Tp-Azo-COF anode material by other organic or inorganic electrode materials. Therefore, the characteristic peak of Tp-Azo-COF has not emerged in the PXRD patterns. More importantly, the assembled LIBs deliver an outstanding electrochemical performance, indicating the excellent structural stability of Tp-Azo-COF, which is in agreement with other reports.^{37,39} Accordingly, the aforementioned analysis can demonstrate the structural stability of N=N- and C=O-linked COFs with enhanced reversibility for the LIBs.

To further understand the fast rate capability, we used the CV technique to study the electrochemical reaction kinetics of Tp-Azo-COF. As illustrated in Figure 4a, the current response (i) versus the scan rate (v , 0.1–1.0 mV s^{-1}) is evaluated. There are continuous changes in peak current density, which should be assigned to the transformation of the diffusion-controlled mechanism to a surface-controlled mechanism and the possible change (partial amorphization) of the crystal structure of the electrode during repetitive cycling. The linear fit of the peak current intensities for CV curves at different scan rates versus the scan rate or the square root of the sweep rate is analyzed in Figure 4b. The slope values for the cathodic peak and anodic peak are calculated to be 0.7 and 0.67, respectively. The slope values are close to 0.5, which implies that the reaction kinetics of Tp-Azo-COF is determined by Li-ion diffusion.^{47,48} The order and extended framework of Tp-Azo-COF show abundant N=N and C=O units that contribute to fast Li-

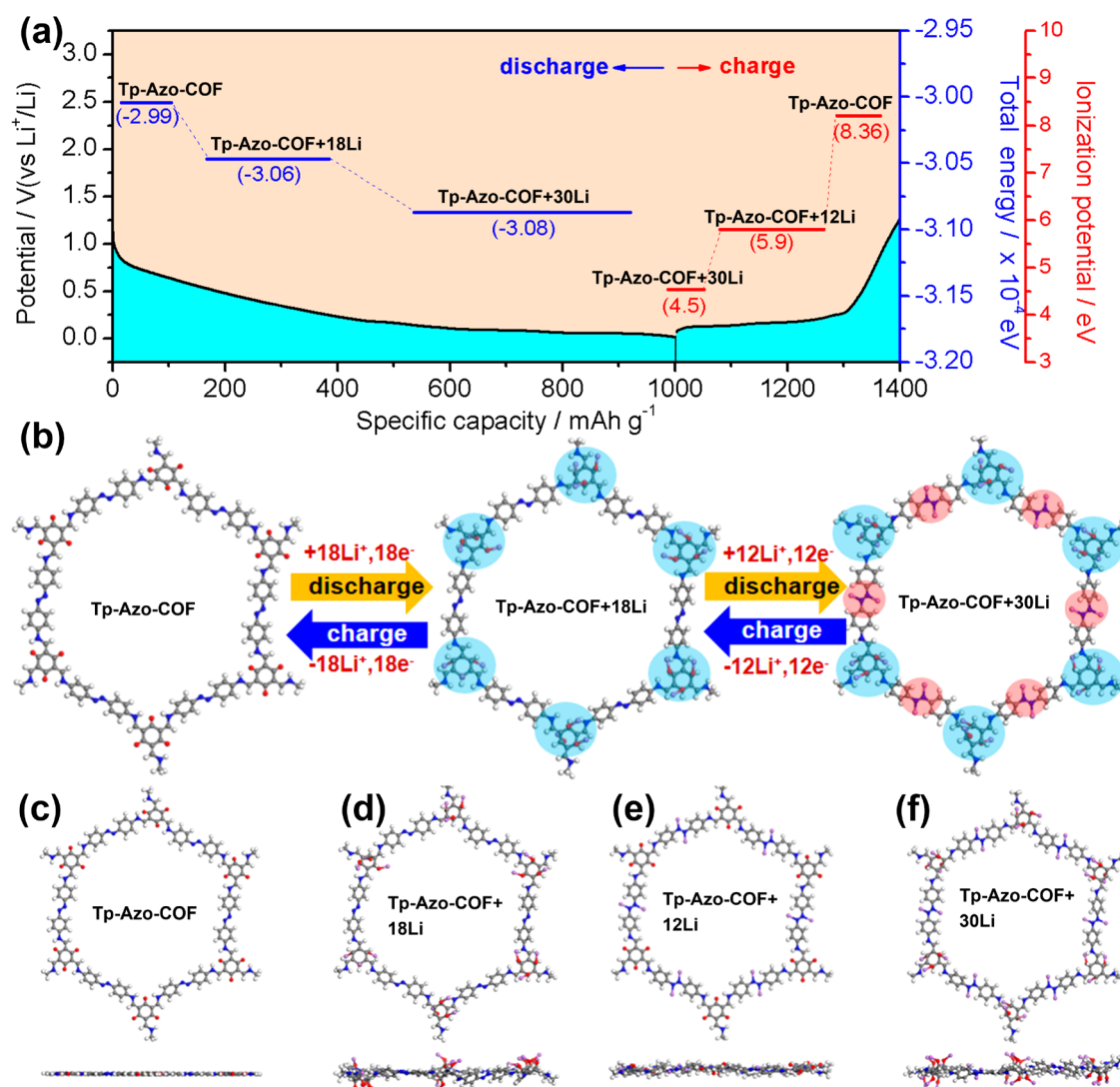


Figure 5. (a) Proposed lithiation pathway for the Tp-Azo-COF electrode. The left axis shows the redox potential vs Li^+/Li , and the right axis shows the total energy and ionization potential of various lithiated Tp-Azo-COF structures. (b) Structural evolution during the lithiation/delithiation procedure. The binding sites between Li and the $\text{C}=\text{O}$ and $\text{N}=\text{N}$ groups are indicated by blue and red spheres, respectively. (c–f) Schematics of the optimized structures of Tp-Azo-COF, Tp-Azo-COF+18Li, Tp-Azo-COF+12Li, and Tp-Azo-COF+30Li, respectively, at different stages of Li.

ion diffusion. Panels c and d of Figure 4 show pseudocapacitive and diffusion-controlled charge storage contributions, and the proportion of the capacitive contribution is increased apparently with the enhancement of the scan rate in the Tp-Azo-COF electrode, revealing Li-ion storage in Tp-Azo-COF is a kinetically fast pseudocapacitive procedure, which is beneficial for the high rate performance of Li-ion batteries.³⁰ Additionally, Figure S9 shows the electrochemical impedance performance of fresh and recycled electrodes (100 cycles). An obvious change in the charge-transfer resistance from 42.3 Ω for the fresh electrode to 24.1 Ω for the recycled electrode can be found, indicating the rapid and stable reaction kinetics of the anode, which is also in line with other reports.^{49,50}

According to analysis presented above, the electrochemical reaction mechanism of Tp-Azo-COF and Li ion is deduced as shown in Figure S10. We propose that Tp-Azo-COF undergoes $\text{C}=\text{O}$ and $\text{N}=\text{N}$ bond reduction during the Li^+ insertion/extraction procedure. Because the O atom is more electronegative than the N atom, the Li^+ insertion reaction will occur at the $\text{C}=\text{O}$ sites, and each $\text{C}=\text{O}$ unit of the β -

ketoenamine receives one Li^+ and forms the lithium alcoholate species.³⁷ In other words, one unit of Tp-Azo-COF can receive 18 Li^+ ions (denoted Tp-Azo-COF+18Li). In addition, one azo group can receive two more Li^+ ions and forms the N–Li species (total of 12 Li^+ ions).^{26,27} With this in mind, one unit of Tp-Azo-COF can receive 30 Li^+ ions during the discharging process (denoted as Tp-Azo-COF+30Li). In the subsequent charging procedure, a reversible reaction occurs and the lithium alcoholate and N–Li species return to $\text{C}=\text{O}$ and $\text{N}=\text{N}$ groups followed by extraction of Li^+ from the active sites.

To better understand the redox mechanism of the Tp-Azo-COF electrode, with multiple lithiation processes, density functional theory (DFT) is used to simulate the lithiation/delithiation processes. The total energy is implemented to explain the intensity of activity¹⁸ and calculated to be -2.99×10^{-4} eV for Tp-Azo-COF, -3.06×10^{-4} eV for Tp-Azo-COF+18Li, and -3.08×10^{-4} eV for Tp-Azo-COF+30Li in the process of lithiation (Figure 5a). Consequently, the total energy difference between fresh Tp-Azo-COF and Tp-Azo-COF+18Li is calculated to be -0.07×10^{-4} eV; this process

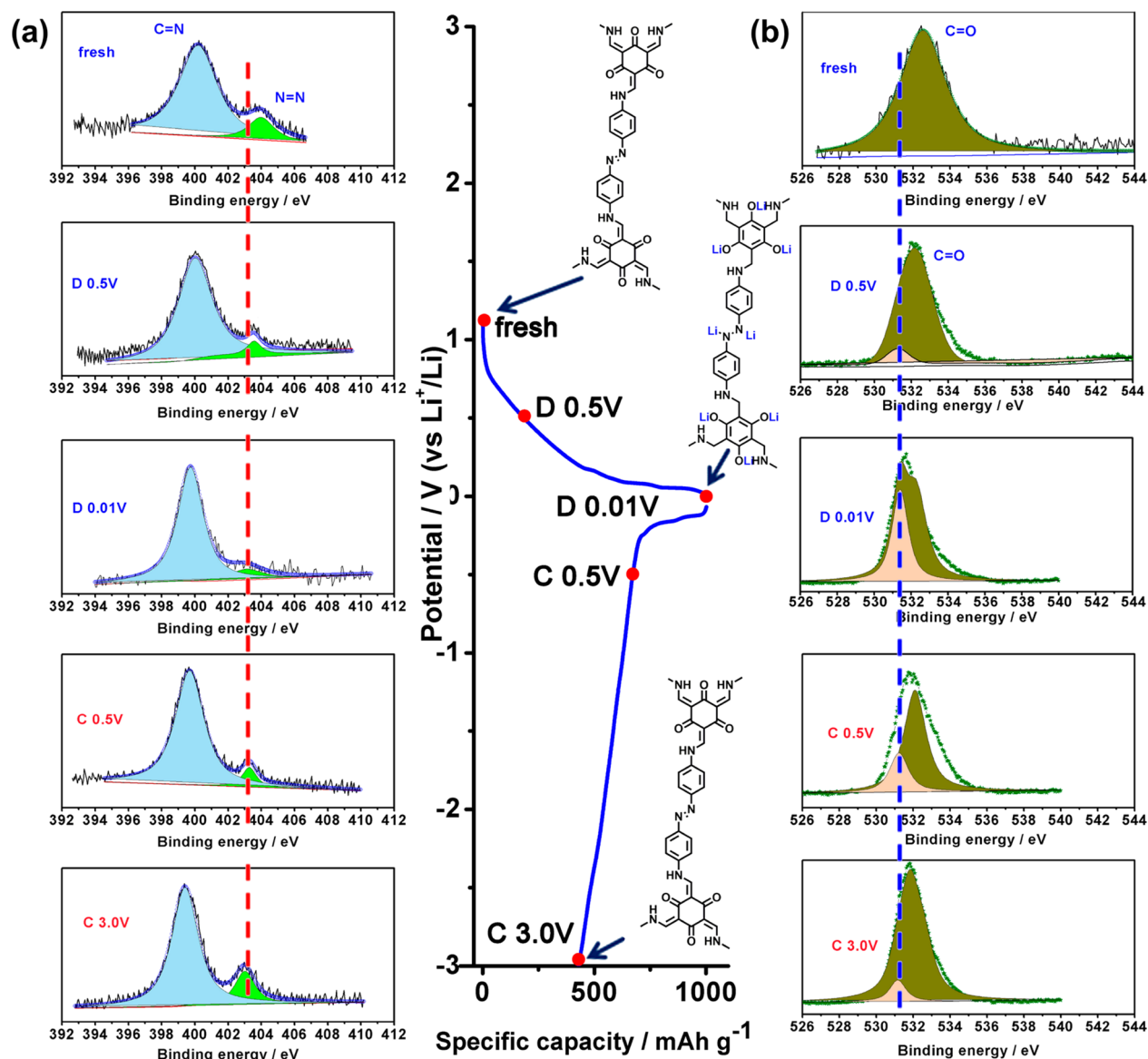


Figure 6. (a) Comparison of XPS spectra of N 1s for a fresh Tp-Azo-COF sample, discharged to 0.5 and 0.01 V and charged to 0.5 and 3.0 V. (b) Comparison of XPS spectra of O 1s for a fresh Tp-Azo-COF sample, discharged to 0.5 and 0.01 V and charged to 0.5 and 3.0 V.

can be assigned to the C=O group in Tp-Azo-COF that reacts with 18 Li atoms. Via a similar analysis, the total energy difference between Tp-Azo-COF+18Li and Tp-Azo-COF+30Li is calculated to be -0.02×10^{-4} eV, and this process is attributed to the N=N group in Tp-Azo-COF+18Li that reacts with 12 additional Li⁺ ions. The total energy difference between fresh Tp-Azo-COF and Tp-Azo-COF+18Li is lower than that between Tp-Azo-COF and Tp-Azo-COF+30Li, implying lithiation of the C=O group is easier than that of the N=N group in the discharging procedure (Figure 5a). In the charging process, the ionization potentials for the deionization of Tp-Azo-COF+30Li, Tp-Azo-COF+12Li, and Tp-Azo-COF are 4.5, 5.9, and 8.36 eV, respectively (Figure 5a). The ionization potential of Tp-Azo-COF+30Li is the lowest, suggesting Tp-Azo-COF-30Li can lose the 18 Li⁺ ions and yield Tp-Azo-COF+12Li, and Tp-Azo-COF+12Li continuously loses the 12 Li⁺ ions to yield the original Tp-Azo-COF. This order in the charging process coincides well with the discharging process, illustrating the Li⁺ preferentially interacts with C=O. Figure 5b can further certify this

discharge–charge procedure. The optimized structures for Tp-Azo-COF, Tp-Azo-COF+18Li, Tp-Azo-COF+12Li, and Tp-Azo-COF+30Li are shown in panels c–f, respectively, of Figure 5. The various energies such as the electronic energy, core–core repulsion, total energy, ionization potential, and heat of formation for each optimized structure are calculated and listed in Table S2. The electronic energies for Tp-Azo-COF, Tp-Azo-COF+18Li, Tp-Azo-COF+12Li, and Tp-Azo-COF+30Li are -4.32×10^{-5} , -4.61×10^{-5} , -4.37×10^{-5} , and -4.7×10^{-5} eV, respectively. The electronic energy for Tp-Azo-COF+18Li is much lower than those of Tp-Azo-COF and Tp-Azo-COF+12Li, which suggests that C=O in Tp-Azo-COF primarily interacts with 18 Li ions. This conclusion is in agreement with the ionization potential. More importantly, the surface electrostatic potentials of Tp-Azo-COF, Tp-Azo-COF+18Li, Tp-Azo-COF+12Li, and Tp-Azo-COF+30Li (Figure S11) can further certify the difference in electronegativity. It is clearly observed that the section of C=O is stronger than the section of N=N, meaning the Li⁺ more easily binds with C=

O than with N=N, which is in good agreement with the total energy, ionization potential, and electronic energy.

XPS is applied to analyze the electrochemical reaction of Li⁺ with the N=N and C=O groups. For the pristine Tp-Azo-COF material, the XPS survey (Figure S12) displays the C, N, and O elements, and high-resolution XPS (HRXPS) of C 1s for Tp-Azo-COF shows the C=C, C-N, and C=O chemical bonds (Figure S13). In addition, HRXPS of O 1s (Figure S14) for Tp-Azo-COF presents the C=O and HRXPS of N 1s (Figure S14) exhibits the N=N and C-N bonds. These results are quite consistent with the chemical structure of Tp-Azo-COF. When the electrode is discharged to 0.01 V, the peak was shifted to the lower binding energy of 403.4 eV and the intensity is reduced, which can be attributed to the consumption of N=N and the formation of the Li-N-N-Li bond after lithium insertion. When Tp-Azo-COF is charged to 3 V, the intensity of the N=N bond can return to the fresh state,^{26–28} which confirms the reversibility of the (de)lithiation processes of an azo-modified COF (Figure 6a). In addition, a similar process can be seen in the XPS spectra of O 1s during the discharge-charge process (Figure 6b). When the Tp-Azo-COF electrode is discharged to 0.5 V, a new peak appears at a binding energy of ~534 eV, which is assigned to the Li-O species, and the intensity increases with a discharge potential at 0.01 V.^{51,52} It is interesting to notice that the intensity of the peak decreases under the charge procedure, suggesting the excellent reversibility of the Tp-Azo-COF electrode.

In summary, Tp-Azo-COF with dual active sites of C=O and N=N was, for the first time, proposed as a novel anode material and successfully applied in Li-ion batteries. Tp-Azo-COF possesses abundant redox-active C=O and N=N centers, a large surface area, and a porous structure, which is beneficial for high capacity output and fast Li storage. It is noticeable that both azo and robust carbonyl units play important roles in enhancing the structural stability of Tp-Azo-COF during the discharging/charging process, making it a reliable and productive anode material for Li storage. The prepared LIBs deliver an excellent specific capability of 305.97 mAh g⁻¹ at a current density of 1000 mA g⁻¹ after 3000 cycles. The mechanism has been closely studied by DFT calculations and in (ex) situ FT-IR, Raman, and XPS characterization, revealing N=N and C=O bonds acted as effective electrochemically active sites during the electrochemical cycling process. The crucial finding of various active centers with the covalent organic framework in our study presents potential benefits for fast Li storage and can be easily continued for other organic electrode schemes with durable cycling stability and reversibility.

■ ASSOCIATED CONTENT

SI Supporting Information

The Supporting Information is available free of charge at <https://pubs.acs.org/doi/10.1021/acseenergylett.0c00069>.

Chemical reagents, characterization, synthetic procedure for Tp-Azo-COF, electrochemical measurements, and other materials (PDF)

■ AUTHOR INFORMATION

Corresponding Authors

Hong Guo – School of Materials Science and Engineering, Yunnan Key Laboratory for Micro/Nano Materials and Technology, Yunnan University, Kunming 650091, China;

orcid.org/0000-0001-5693-2980; Email: guohongcom@126.com

Xueliang Sun – Nanomaterials and Energy Lab, Department of Mechanical and Materials Engineering, Western University, London, Ontario N6A 5B9, Canada; orcid.org/0000-0003-0374-1245; Email: xsun9@uwo.ca

Authors

Genfu Zhao – School of Materials Science and Engineering, Yunnan Key Laboratory for Micro/Nano Materials and Technology, Yunnan University, Kunming 650091, China

Yuhao Zhang – School of Materials Science and Engineering, Yunnan Key Laboratory for Micro/Nano Materials and Technology, Yunnan University, Kunming 650091, China

Zhihui Gao – School of Materials Science and Engineering, Yunnan Key Laboratory for Micro/Nano Materials and Technology, Yunnan University, Kunming 650091, China

Huani Li – School of Materials Science and Engineering, Yunnan Key Laboratory for Micro/Nano Materials and Technology, Yunnan University, Kunming 650091, China

Shuming Liu – School of Materials Science and Engineering, Yunnan Key Laboratory for Micro/Nano Materials and Technology, Yunnan University, Kunming 650091, China

Sheng Cai – School of Materials Science and Engineering, Yunnan Key Laboratory for Micro/Nano Materials and Technology, Yunnan University, Kunming 650091, China

Xiaofei Yang – Nanomaterials and Energy Lab, Department of Mechanical and Materials Engineering, Western University, London, Ontario N6A 5B9, Canada

Complete contact information is available at:

<https://pubs.acs.org/10.1021/acsenergylett.0c00069>

Author Contributions

[§]G.Z. and Y.Z. contributed equally to this work.

Notes

The authors declare no competing financial interest.

■ ACKNOWLEDGMENTS

The authors acknowledge financial support provided by the Key National Natural Science Foundation of Yunnan Province (2018FA028 and 2019FY003023), the National Natural Science Foundation of China (51474191 and 21467030), the Major State Basic Research Development Program of China (973 Program, 2014CB643406), and the Program for Outstanding Young Talents (2018) of Yunnan University.

■ REFERENCES

- (1) Xu, K. Electrolytes and Interphases in Li-Ion Batteries and Beyond. *Chem. Rev.* **2014**, *114*, 11503–11618.
- (2) Li, X.; Liang, J.; Luo, J.; Norouzi Banis, M.; Wang, C.; Li, W.; Deng, S.; Yu, C.; Zhao, F.; Hu, Y.; Sham, T.-K.; Zhang, L.; Zhao, S.; Lu, S.; Huang, H.; Li, R.; Adair, K. R.; Sun, X. Air-Stable Li₃InCl₆ Electrolyte with High Voltage Compatibility for All-Solid-State Batteries. *Energy Environ. Sci.* **2019**, *12*, 2665–2671.
- (3) Guo, H.; Li, T.; Chen, W.; Liu, L.; Yang, X.; Wang, Y.; Guo, Y. General Design of Hollow Porous CoFe₂O₄ Nanocubes from Metal-Organic Frameworks with Extraordinary Lithium Storage. *Nanoscale* **2014**, *6*, 15168–15174.
- (4) Xu, F.; Yang, S.; Chen, X.; Liu, Q.; Li, H.; Wang, H.; Wei, B.; Jiang, D. Energy-Storage Covalent Organic Frameworks: Improving Performance via Engineering Polysulfide Chains on Walls. *Chem. Sci.* **2019**, *10*, 6001–6006.

- (5) Larcher, D.; Tarascon, J. M. Towards Greener and more Sustainable Batteries for Electrical Energy Storage. *Nat. Chem.* **2015**, *7*, 19–29.
- (6) Wang, W.; Guo, Y.; Liu, L.; Wang, S.; Yang, X.; Guo, H. Gold Coating for a High Performance $\text{Li}_4\text{Ti}_5\text{O}_{12}$ Nanorod Aggregates Anode in Lithium-Ion Batteries. *J. Power Sources* **2014**, *245*, 624–629.
- (7) Schon, T. B.; McAllister, B. T.; Li, P. F.; Seferos, D. S. The Rise of Organic Electrode Materials for Energy Storage. *Chem. Soc. Rev.* **2016**, *45*, 6345–6404.
- (8) Liang, Y.; Tao, Z.; Chen, J. Organic Electrode Materials for Rechargeable Lithium Batteries. *Adv. Energy Mater.* **2012**, *2*, 742–769.
- (9) Back, J.; Park, J.; Kim, Y.; Kang, H.; Kim, Y.; Park, M. J.; Kim, K.; Lee, E. Triazenyl Radicals Stabilized by N-Heterocyclic Carbenes. *J. Am. Chem. Soc.* **2017**, *139*, 15300–15303.
- (10) Janoschka, T.; Teichler, A.; Häupler, B.; Jähnert, T.; Hager, M. D.; Schubert, U. S. Reactive Inkjet Printing of Cathodes for Organic Radical Batteries. *Adv. Energy Mater.* **2013**, *3*, 1025–1028.
- (11) Liang, Y.; Jing, Y.; Gheyhani, S.; Lee, K.-Y.; Liu, P.; Facchetti, A.; Yao, Y. Universal Quinone Electrodes for Long Cycle Life Aqueous Rechargeable Batteries. *Nat. Mater.* **2017**, *16*, 841–848.
- (12) Lee, M.; Hong, J.; Lopez, J.; Sun, Y.; Feng, D.; Lim, K.; Chueh, W. C.; Toney, M. F.; Cui, Y.; Bao, Z. High-Performance Sodium Organic Battery by Realizing Four-Sodium Storage in Disodium Rhodizonate. *Nat. Energy* **2017**, *2*, 861–868.
- (13) Li, Y.; Lu, Y.; Zhao, C.; Hu, Y.-S.; Titirici, M.-M.; Li, H.; Huang, X.; Chen, L. Recent Advances of Electrode Materials for Low-cost Sodium-ion Batteries towards Practical Application for Grid Energy Storage. *Energy Storage Mater.* **2017**, *7*, 130–151.
- (14) Zhang, J.; Sun, B.; Zhao, Y.; Kretschmer, K.; Wang, G. Modified Tetrathiafulvalene as an Organic Conductor for Improving Performances of $\text{Li}@\text{O}_2$ Batteries. *Angew. Chem., Int. Ed.* **2017**, *56*, 8505–8509.
- (15) Zhao, Q.; Wang, J.; Lu, Y.; Li, Y.; Liang, G.; Chen, J. Oxocarbon Salts for Fast Rechargeable Batteries. *Angew. Chem., Int. Ed.* **2016**, *55*, 12528–12532.
- (16) Han, C.; Li, H.; Shi, R.; Zhang, T.; Tong, J.; Li, J.; Li, B. Organic Quinones towards Advanced Electrochemical Energy Storage: Recent Advances and Challenges. *J. Mater. Chem. A* **2019**, *7*, 23378–23415.
- (17) Song, Z.; Qian, Y.; Gordin, M. L.; Tang, D.; Xu, T.; Otani, M.; Zhan, H.; Zhou, H.; Wang, D. Polyanthraquinone as a Reliable Organic Electrode for Stable and Fast Lithium Storage. *Angew. Chem., Int. Ed.* **2015**, *54*, 13947–13951.
- (18) Peng, C.; Ning, G.-H.; Su, J.; Zhong, G.; Tang, W.; Tian, B.; Su, C.; Yu, D.; Zu, L.; Yang, J.; Ng, M.-F.; Hu, Y.-S.; Yang, Y.; Armand, M.; Loh, K. P. Reversible Multi-Electron Redox Chemistry of π -Conjugated Ncontaining Heteroaromatic Molecule-Based Organic Cathodes. *Nat. Energy* **2017**, *2*, 17074–17082.
- (19) Lee, M.; Hong, J.; Seo, D. H.; Nam, D. H.; Nam, K. T.; Kang, K.; Park, C. B. Redox Cofactor from Biological Energy Transduction as Molecularly Tunable Energy-Storage Compound. *Angew. Chem., Int. Ed.* **2013**, *52*, 8322–8328.
- (20) Hong, J.; Lee, M.; Lee, B.; Seo, D.-H.; Park, C. B.; Kang, K. Biologically Inspired Pteridine Redox Centres for Rechargeable Batteries. *Nat. Commun.* **2014**, *5*, 5335–5344.
- (21) Zhang, C.; He, Y.; Mu, P.; Wang, X.; He, Q.; Chen, Y.; Zeng, J.; Wang, F.; Xu, Y.; Jiang, J.-X. Toward High Performance Thiophene Containing Conjugated Microporous Polymer Anodes for Lithium Ion Batteries through Structure Design. *Adv. Funct. Mater.* **2018**, *28*, 1705432–1705440.
- (22) Wang, S.; Wang, Q.; Shao, P.; Han, Y.; Gao, X.; Ma, L.; Yuan, S.; Ma, X.; Zhou, J.; Feng, X.; Wang, B. Exfoliation of Covalent Organic Frameworks into Few-Layer Redox-Active Nanosheets as Cathode Materials for Lithium-Ion Batteries. *J. Am. Chem. Soc.* **2017**, *139*, 4258–4261.
- (23) See, K. A.; Hug, S.; Schwinghammer, K.; Lumley, M. A.; Zheng, Y.; Nolt, J. M.; Stucky, G. D.; Wudl, F.; Lotsch, B. V.; Seshadri, R. Lithium Charge Storage Mechanisms of Cross-Linked Triazine Networks and Their Porous Carbon Derivatives. *Chem. Mater.* **2015**, *27*, 3821–3829.
- (24) Wei, X.; Xu, W.; Vijayakumar, M.; Cosimbescu, L.; Liu, T.; Sprenkle, V.; Wang, W. TEMPO-Based Catholyte for High-Energy Density Nonaqueous Redox Flow Batteries. *Adv. Mater.* **2014**, *26*, 7649–7653.
- (25) Guo, W.; Yin, Y.-X.; Xin, S.; Guo, Y.-G.; Wan, L.-J. Superior Radical Polymer Cathode Material with a two-Electron Process Redox Reaction Promoted by Graphene. *Energy Environ. Sci.* **2012**, *5*, 5221–5225.
- (26) Weeraratne, K. S.; Alzharani, A. A.; El-Kaderi, H. M. Redox-Active Porous Organic Polymers as Novel Electrode Materials for Green Rechargeable Sodium-Ion Batteries. *ACS Appl. Mater. Interfaces* **2019**, *11*, 23520–23526.
- (27) Luo, C.; Borodin, O.; Ji, X.; Hou, S.; Gaskell, K. J.; Fan, X.; Chen, J.; Deng, T.; Wang, R.; Jiang, J.; Wang, C. Azo Compounds as a Family of Organic Electrode Materials for Alkali-Ion Batteries. *Proc. Natl. Acad. Sci. U. S. A.* **2018**, *115*, 2004–2009.
- (28) Luo, C.; Xu, G.-L.; Ji, X.; Hou, S.; Chen, L.; Wang, F.; Jiang, J.; Chen, Z.; Ren, Y.; Amine, K.; Wang, C. Reversible Redox Chemistry of Azo Compounds for Sodium-Ion Batteries. *Angew. Chem., Int. Ed.* **2018**, *57*, 2879–2883.
- (29) Sun, D.; Rosokha, S. V.; Kochi, J. K. Donor-Acceptor (Electronic) Coupling in the Precursor Complex to Organic Electron Transfer: Intermolecular and Intramolecular Self-Exchange between Phenothiazine Redox Centers. *J. Am. Chem. Soc.* **2004**, *126*, 1388–1401.
- (30) Zhao, Q.; Lu, Y.; Chen, J. Advanced Organic Electrode Materials for Rechargeable Sodium-Ion Batteries. *Adv. Energy Mater.* **2017**, *7*, 1601792–1601813.
- (31) Cote, A. P.; Benin, A. I.; Ockwig, N. W.; O'keeffe, M.; Matzger, A. J.; Yaghi, O. M. Porous, Crystalline, Covalent Organic Frameworks. *Science* **2005**, *310*, 1166–1170.
- (32) Ding, S.-Y.; Wang, W. Covalent Organic Frameworks (COFs): From Design to Applications. *Chem. Soc. Rev.* **2013**, *42*, 548–568.
- (33) Kandambeth, S.; Dey, K.; Banerjee, R. Covalent Organic Frameworks: Chemistry beyond the Structure. *J. Am. Chem. Soc.* **2019**, *141*, 1807–1822.
- (34) Zhao, X.; Pachfule, P.; Li, S.; Langenhahn, T.; Ye, M.; Schlesiger, C.; Praetz, S.; Schmidt, J.; Thomas, A. Macro/Microporous Covalent Organic Frameworks for Efficient Electrocatalysis. *J. Am. Chem. Soc.* **2019**, *141*, 6623–6630.
- (35) Jeong, K.; Park, S.; Jung, G. Y.; Kim, S. H.; Lee, Y.-H.; Kwak, S. K.; Lee, S.-Y. Solvent-Free, Single Lithium-Ion Conducting Covalent Organic Frameworks. *J. Am. Chem. Soc.* **2019**, *141*, 5880–5885.
- (36) Halder, A.; Ghosh, M.; Khayum, M. A.; Bera, S.; Addicoat, M.; Sasmal, H. S.; Karak, S.; Kurungot, S.; Banerjee, R. Interlayer Hydrogen-Bonded Covalent Organic Frameworks as High-Performance Supercapacitors. *J. Am. Chem. Soc.* **2018**, *140*, 10941–10945.
- (37) Gu, S.; Wu, S.; Cao, L.; Li, M.; Qin, N.; Zhu, J.; Wang, Z.; Li, Y.; Li, Z.; Chen, J.; Lu, Z. Tunable Redox Chemistry and Stability of Radical Intermediates in 2D Covalent Organic Frameworks for High Performance Sodium Ion Batteries. *J. Am. Chem. Soc.* **2019**, *141*, 9623–9628.
- (38) Wang, G.; Chandrasekhar, N.; Biswal, B. P.; Becker, D.; Paasch, S.; Brunner, E.; Addicoat, M.; Yu, M.; Berger, R.; Feng, X. A Crystalline, 2D Polyarylimide Cathode for Ultrastable and Ultrafast Li storage. *Adv. Mater.* **2019**, *31*, 1901478–1901483.
- (39) Chandra, S.; Kundu, T.; Kandambeth, S.; BabaRao, R.; Marathe, Y.; Kunjir, S. M.; Banerjee, R. Phosphoric Acid Loaded Azo (-N = N-) Based Covalent Organic Framework for Proton Conduction. *J. Am. Chem. Soc.* **2014**, *136*, 6570–6573.
- (40) Karak, S.; Kandambeth, S.; Biswal, B. P.; Sasmal, H. S.; Kumar, S.; Pachfule, P.; Banerjee, R. Constructing Ultraporous Covalent Organic Frameworks in Seconds via an Organic Terracotta Process. *J. Am. Chem. Soc.* **2017**, *139*, 1856–1862.
- (41) Chen, X.; Li, Y.; Wang, L.; Xu, Y.; Nie, A.; Li, Q.; Wu, F.; Sun, W.; Zhang, X.; Vajtai, R.; Ajayan, P. M.; Chen, L.; Wang, Y. High-

Lithium-Affinity Chemically Exfoliated 2D Covalent Organic Frameworks. *Adv. Mater.* **2019**, *31*, 1901640–1901647.

(42) Lu, S.; Hu, Y.; Wan, S.; McCaffrey, R.; Jin, Y.; Gu, H.; Zhang, W. Synthesis of Ultrafine and Highly Dispersed Metal Nanoparticles Confined in a Thioether-Containing Covalent Organic Framework and Their Catalytic Applications. *J. Am. Chem. Soc.* **2017**, *139*, 17082–17088.

(43) Zhang, G.; Hong, Y.; Nishiyama, Y.; Bai, S.; Kitagawa, S.; Horike, S. Accumulation of Glassy Poly(ethylene oxide) Anchored in a Covalent Organic Framework as a Solid-State Li⁺ Electrolyte. *J. Am. Chem. Soc.* **2019**, *141*, 1227–1234.

(44) DeBlase, C. R.; Silberstein, K. E.; Truong, T.-T.; Abruña, H. D.; Dichtel, W. R. β -Ketoenamine-Linked Covalent Organic Frameworks Capable of Pseudocapacitive Energy Storage. *J. Am. Chem. Soc.* **2013**, *135*, 16821–16824.

(45) Stuart, C. M.; Frontiera, R. R.; Mathies, R. A. Excited-State Structure and Dynamics of Cis- and Trans-Azobenzene from Resonance Raman Intensity Analysis. *J. Phys. Chem. A* **2007**, *111*, 12072–12080.

(46) Liu, H.; Guo, H.; Liu, B.; Liang, M.; Lv, Z.; Adair, K. R.; Sun, X. Few-Layer MoSe₂ Nanosheets with Expanded (002) Planes Confined in Hollow Carbon Nanospheres for Ultrahigh-Performance Na-Ion Batteries. *Adv. Funct. Mater.* **2018**, *28*, 1707480–1707488.

(47) Wang, C.; Xu, Y.; Fang, Y.; Zhou, M.; Liang, L.; Singh, S.; Zhao, H.; Schober, A.; Lei, Y. Extended π -Conjugated System for Fast-Charge and -Discharge Sodium-Ion Batteries. *J. Am. Chem. Soc.* **2015**, *137*, 3124–3130.

(48) Augustyn, V.; Come, J.; Lowe, M. A.; Kim, J. W.; Taberna, P.-L.; Tolbert, S. H.; Abruña, H. D.; Simon, P.; Dunn, B. High-rate electrochemical energy storage through Li⁺ intercalation pseudocapacitance. *Nat. Mater.* **2013**, *12*, 518–522.

(49) Xu, S.; Wang, G.; Biswal, B. P.; Addicoat, M.; Paasch, S.; Sheng, W.; Zhuang, X.; Brunner, E.; Heine, T.; Berger, R.; Feng, X. A Nitrogen-Rich 2D sp²-Carbon-Linked Conjugated Polymer Framework as a High-Performance Cathode for Lithium-Ion Batteries. *Angew. Chem., Int. Ed.* **2019**, *58*, 849–853.

(50) Wu, M.; Zhao, Y.; Sun, B.; Sun, Z.; Li, C.; Han, Y.; Xu, L.; Ge, Z.; Ren, Y.; Zhang, M.; Zhang, Q.; Lu, Y.; Wang, W.; Ma, Y.; Chen, Y. A 2D Covalent Organic Framework as a High-Performance Cathode Material for Lithium-Ion Batteries. *Nano Energy* **2020**, *70*, 104498–104505.

(51) Wang, Y.; Ding, Y.; Pan, L.; Shi, Y.; Yue, Z.; Shi, Y.; Yu, G. Understanding the Size-Dependent Sodium Storage Properties of Na₂C₆O₆-Based Organic Electrodes for Sodium-Ion Batteries. *Nano Lett.* **2016**, *16*, 3329–3334.

(52) Yang, J.; Ju, Z.; Jiang, Y.; Xing, Z.; Xi, B.; Feng, J.; Xiong, S. Enhanced Capacity and Rate Capability of Nitrogen/Oxygen Dual-Doped Hard Carbon in Capacitive Potassium-Ion Storage. *Adv. Mater.* **2018**, *30*, 1700104–1700114.